Review Copy (Rough)
For Presentation at the 1983 Intersociety Energy Conversion Engineering Conference

MITG POST-TEST ANALYSIS AND DESIGN IMPROVEMENTS

A. Schock

Fairchild Space Company
Germantown, Maryland 20874

Abstract

The design, performance analysis, and key attributes of the Modular Isotopic Thermoelectric Generator (MITG) were described in a 1981 IECEC paper; and the design, fabrication, and testing of prototypical MITG test assemblies were described in preceding papers in these proceedings. Each test assembly simulated a typical modular slice of the flight generator.

The present paper describes a detailed thermal-stress analysis, which identified the causes of stress-related problems observed during the tests. It then describes how additional analyses were used to evaluate design changes to alleviate those problems. Additional design improvements are discussed in the next paper in these proceedings, which also describes revised fabrication procedures and updated performance estimates for the generator.

1. Introduction

The design of the Modular Isotopic Thermoelectric Generator (MITG), consisting of identical modular generator slices, was described [1] by the author at the 1981 Intersociety Energy Conversion Engineering Conference (IECEC). Since it offered a number of desirable features and a much higher power-to-weight ratio than current RTGs, DOE initiated a program to build and test such prototypical generator slices, primarily to measure their power output and efficiency, and to determine their performance reproducibility and long-term stability.

The design and fabrication of the initial test assemblies are discussed in a previous paper [2] in these proceedings; and the test plan, methodology, instrumentation, computer control and data acquisition systems, and initial test results are described in the preceding paper [3].

The present paper describes a serious thermal-stress problem revealed by the tests, and presents a detailed structural analysis which identified its causes. Based on the understanding gained, the paper then discusses a number of design modifications, and presents analyses demonstrating their effectiveness in relieving the observed thermal-stress problem.

In addition, the next paper in these proceedings [4] describes some alternative design changes for eliminating the observed thermal-stress problems, and for improving thermal conductance and hermetic sealing between the generator housing and the multicouple cold ends. These design changes have been validated analytically, and are now undergoing experimental confirmation.

Finally, based on these design changes and on updated thermoelectric properties measured at various laboratories during the past two years, that paper describes a revised MITG design and fabrication procedure, presents power and weight predictions for that design, and compares these with similar predictions made in 1981.

2. Test Results

As explained in Reference [3], two tests were carried out, each using the test assembly design depicted in Figure 1.

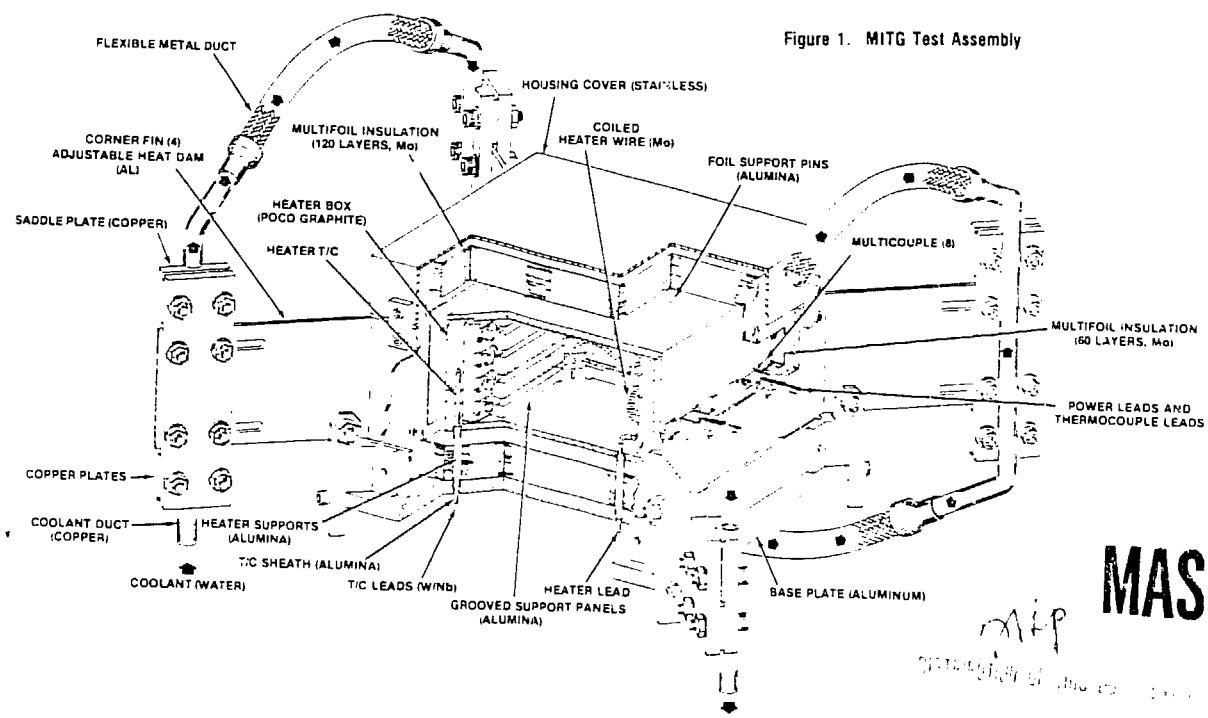

Figure 1. MITG Test Assembly

As shown, each test assembly contains eight multicouples, consisting of 18 series-connected thermoelectric couples. Figure 2 shows an exploded view of a typical multicouple used in these tests. Details of the multicouple design and fabrication procedure are described in Reference [2].

Figure 2. Exploded View of Multicouple

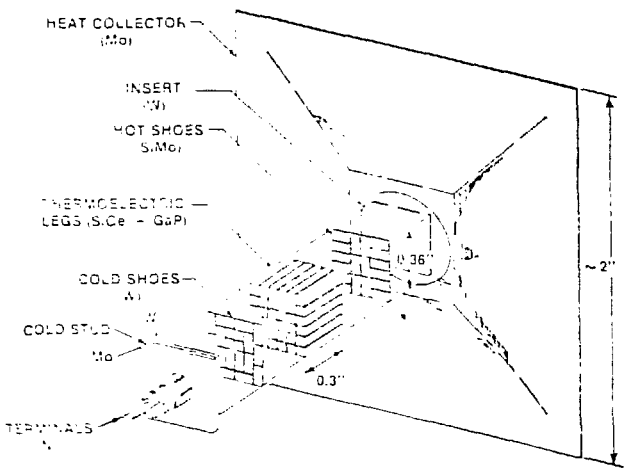

The tests and post-test analyses indicated that the initial multicouple design had a number of problems requiring corrective action. The paper will explain how additional analyses and other studies served to identify the causes of those problems, and to suggest changes in design and fabrication to eliminate them. These changes have been analytically and experimentally evaluated, with very encouraging results. Additional experimental confirmation tests now under way will be described, and their results will be presented at the conference.

3. Thermal-Stress Problem

As reported in Reference [3], even during the outgassing and heat-up of the two test assemblies to their design temperatures, a number of electrical and thermal anomalies became apparent. These appeared to a greater or lesser degree in all 16 multicouples. It was surmised that these anomalies were due to cracks, either within the leg assemblies or in the hot- or cold-shoes; but this could not be confirmed until the tests were terminated.

After disassembly and detailed post-test examinations conducted at Fairchild and in greater detail at a number of other laboratories (Thermo Electron, Battelle-Columbus, Ames, GE-Valley Forge, and Teledyne-Timonium), cracks were found at the following locations:

- Near the center of the cold ends of the leg assemblies
- At the outer edges of their hot ends
- At the outer corners of the cold ends

The first of these was by far the most common and most serious. Such cracks were found in all 16 multicouples, and in many cases had led to complete cleavage at the thermopile's cold end. As shown in Figure 3, the cleaved surface was slightly dome-shaped, concave when viewed from the cold end.

Figure 3. Typical Break at Cold End of Thermopile

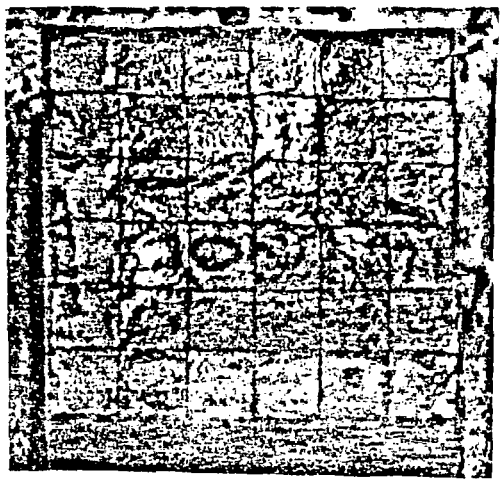

This type of cracking and/or cleavage occurred mostly within the SiGe legs. Thus, it appears that the bonds between the legs and the cold shoes, as well as the glass bonds between the cold shoes and the cold studs, are actually stronger than the SiGe legs themselves.

The second type of crack, near the hot ends' outer edges, occurred much less frequently. When they did occur, these were incipient cracks which did not penetrate far toward the center. In no case did they lead to cleavage or loss of the heat collector.

The third type of crack, near the cold ends' outer corners, appeared even less frequently. The only noticeable evidence of their occurrence was occasional discoloration at the corners of the cleavage planes. This suggested that cracking at the corners may have occurred during fabrication or early during outgassing, whereas the cleanliness of the rest of the broken surface indicated that cleavage had occurred much later, at a higher temperature.

The above-described cracking, particularly the first type, is very serious and must be eliminated. It was considered most likely that the observed cracks were produced by thermal stresses resulting from one or more of the following causes:

- The bimetallic (W/Mo) cold stud, causing bowing during cooldown and heatup after fabrication
- Mismatch in thermal expansion coefficient between the thermoelectric leg assembly and the cold stud and heat collector
- Bowing of the leg assembly's hot and cold ends due to the large (700°C) temperature gradient at operating condition
- The high expansion coefficient of the aluminum wall on which the multicouple is mounted

Each of the above would produce thermal stresses, during fabrication and/or operation, and could be a plausible cause of the observed cracking. Clearly, a detailed stress analysis was needed, covering the thermal history of the multicouple during the various fabrication steps and subsequent heatup to operating temperature. This analysis could identify the dominant cause of thermal stresses. Only then could appropriate design modifications be proposed and evaluated.

4. Thermal Stress Analysis

The model initially used in Fairchild's thermal stress analyses is shown in Figure 4. It represents a 45° segment, taking advantage of the multicouple's eight-fold symmetry. The model included the tungsten heat collector insert, the glass-bonded SiGe leg assembly, the W/Mo cold stud, the Al housing wall, and a nut (which was assumed to be infinitely stiff). The SiMo hot shoes were not modeled separately, but were incorporated in the SiGe leg assembly. Nor were the thin tungsten cold shoes explicitly represented.

Figure 4. Thermal-Stress Model, Base Case

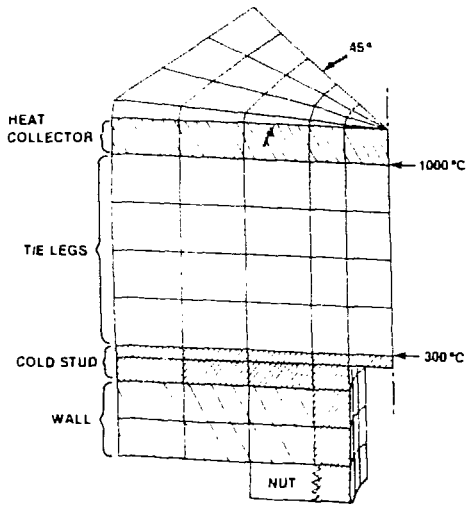

As explained in Reference [5], the analysis made use of the MacNeal-Schwendler version of the NASTRAN computer code, supplemented by the PATRAN pre- and post-processing software of PDA Engineering. A special scheme for accommodating temperature-dependent expansion coefficients was developed by Fairchild. The NASTRAN model contained 144 solid-shell elements connecting 1290 grid points, for a total of 3000 static degrees of freedom. Both 20-node hexahedral elements and 15-node pentahedral elements were used.

Each case analyzed consisted of seven to nine subcases. As explained in [5], these subcases were needed to simulate the thermal cycles involved in brazing the bimetallic cold stud at 980°C, making a high-temperature (1100°C) glass bond between the thermopile and the heat collector, making a low-temperature (680°C) glass bond between the thermopile and the cold stud, bolting the multicouple to the aluminum housing, and heating the assembly to its 1000°C/300°C operating temperature.

A typical case required three to four hours of CPU time, and generated over 80,000 lines of output data. Ultimately, more than 25 cases were analyzed to identify the dominant cause of thermal stresses and to evaluate a variety of possible design fixes.

To reduce the flood of output data to tractable form, a post-processing program was written to extract only the most significant data. First, attention was restricted to stresses in the SiGe leg assembly, since that is where the cracks had occurred. Next, attention was confined to the diagonal boundary plane, since that is where the highest stresses were found to occur. Finally, within that plane, we restricted our attention to the six mesh points at the upper and lower boundaries of the legs, since that is where cracks had been observed and where calculated stresses were highest. By thus restricting our attention, the number of data sets to be examined was reduced from 1290 mesh points to 12 mesh points.

The computed results for those 12 mesh point are displayed in Table 1, which presents both the fabrication stresses, after cooldown, and the operating stresses with the 1000°C/300°C temperature gradient.

The data presented are for the base case; i.e., the case representing the multicouple design in the initial test assemblies. Note that all stresses have been rounded off to the nearest ksi. Although this often leaves only one significant figure, the resultant clarity makes it much easier to discern trends and differences between alternative designs.

Table 1. Base Case
Tensile Stresses in SiGe, in ksi

TENSILE STRESSES IN SiGe, IN ksi

CASE #			1					
Housing Wall			Al					
SiGe Exp Coeff			$\alpha(T)$					
Cold Stud Material			W/Mo					
Cold Stud Thickness (mil)			10/20					
Heat Collector Material			W					
Heat Collector Thickness (mil)			60					
		Radial Position	Cartesian Stresses σ_x	σ_y	σ_z	Principal Stresses σ_A	σ_B	σ_C
AFTER FABRICATION	Hot End	1	-15	-15	-3	-3	-17	-14
		2	-15	-5	-8	-4	-9	-5
		3	-13	-12	-3	-2	-14	-11
		4	-12	-12	-2	0	-14	-11
		5	-12	-13	0	3	-16	-13
		6	-14	-19	3	2	-20	-13
	Cold End	1	-13	-13	1	1	-14	-13
		2	-14	-13	-3	-2	-15	-13
		3	-15	-15	-3	-3	-16	-14
		4	-15	-14	-2	0	-17	-13
		5	-14	-14	-1	-1	-17	-14
		6	-11	-16	1	1	-16	-12
IN OPERATION	Hot End	1	-7	-7	-2	-1	-8	-2
		2	-3	-2	-5	-2	-4	-1
		3	-5	-5	-1	-1	-6	-2
		4	-5	-5	-2	-1	-6	-1
		5	-4	-4	-2	0	-5	-1
		6	-1	-2	5	6	-3	-1
	Cold End	1	0	0	2	2	-1	0
		2	-4	-7	17	17	-8	-4
		3	-7	-4	10	14	-9	-6
		4	-8	-4	-5	-1	-9	-8
		5	-7	-6	-3	-2	-8	-6
		6	-5	-7	0	0	-8	-5

Table 1 presents both the cartesian stresses and the principal stresses. As can be seen, the highest cartesian tensile stresses (σ_z) are in the z-direction, parallel to the multicouple axis; and these are very close to the largest principal stresses (σ_A). Consequently, our examination of future results can be further simplified by confining our attention to the axial tensile stresses at the critical 12 mesh points. This is illustrated in Table 2, for the base case.

CASE #	1	
Housing Wall	Al	
SiGe Exp Coeff	$\alpha(T)$	
Cold Stud Material	W/Mo	
Cold Stud Thickness (mil)	10/20	
Heat Collector Material	W	
Heat Collector Thickness (mil)	60	
	Radial Position	
AFTER FABRICATION — Hot End	1	-3
	2	-8
	3	-3
	4	-2
	5	1
	6	3
AFTER FABRICATION — Cold End	1	1
	2	-3
	3	-3
	4	-2
	5	1
	6	7
IN OPERATION — Hot End	1	-2
	2	-5
	3	-1
	4	-2
	5	2
	6	5
IN OPERATION — Cold End	1	2
	2	17
	3	10
	4	-5
	5	-3
	6	3

Table 2. Base Case
Axial Tensile Stresses in SiGe, in ksi

← High fabrication stress at outer corner of cold end

← High operating stress at outer corner of hot end

← Very high operating stress near center of cold end

The most interesting thing about Table 2 is how closely the analytical results match the experimental findings. The worst stress is the 17 ksi operating stress near the center of the leg assembly's cold end, precisely where the dome-shaped cleavages had occurred. The operating stress at the outer corner of the hot end and the fabrication stress at the corner of the cold end are lower, but still too high. These are the locations where secondary damage was observed in the tests. This excellent agreement between the experimental and analytical results lends confidence in the validity of the analytical model and methodology.

The analytical results for the base case are displayed graphically in Figure 5. This, and similar figures presented later, shows (in exaggerated form) the deflections due to the operational temperature gradients. Note the curvature of the upper and lower faces of the SiGe assembly, as predicted by theory, and also the thermal expansion of the aluminum wall.

Figure 5. Base Case

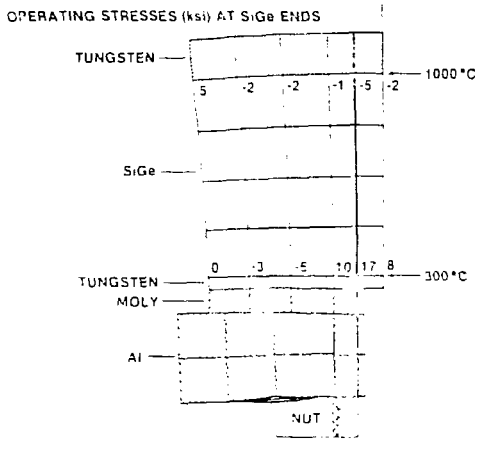

The figure also shows the axial stresses at the 12 critical points under operating conditions (in ksi). The latter are obtained by superposition of the fabrication and temperature-gradient stresses.

5. Dominant Source of Thermal Stresses

Having gained confidence in the validity of the analysis, the model was next used to identify the dominant source(s) of the thermal stresses, and to evaluate design modifications to eliminate or substantially reduce those stresses. The four possible causes of thermal stress listed at the end of Section 3 were investigated one at a time.

5.1 Bimetallic Cold Stud

First, we analyzed a case identical to the base case except for the use of an all-tungsten cold stud. This was to eliminate the effect of the bimetallic cold stud, which would tend to change its curvature when it was heated or cooled. The results of that change are presented in Table 3 (Case 3).

As shown, elimination of the bimetallic cold stud reduces the fabrication stress at the cold end's corners from 8 ksi to 1 ksi. But it does nothing to reduce the worst problem, the very high operating stress near the center of the cold end. In fact, that stress actually went up a little, probably because of the higher modulus of tungsten.

Table 3. Effect of Bi-Metallic Cold Stud

AXIAL TENSILE STRESSES IN SiGe (IN KSI)

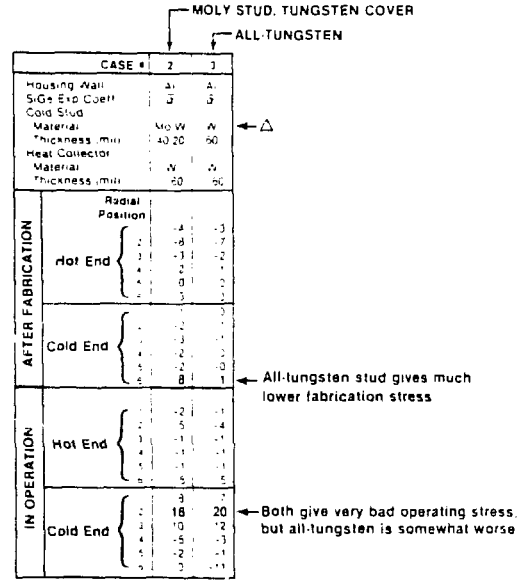

5.2 Mismatched Expansion Coefficients

The second possible cause investigated was the difference in expansion coefficients between SiGe and tungsten. Although these two materials are very close, tungsten does have a slightly higher coefficient. To eliminate this effect, a case was run in which the expansion coefficient of tungsten was arbitrarily set equal to that of SiGe. The resultant stresses are shown in Table 4 (Case 4).

Table 4. Effect of Matched Expansion Coefficients

AXIAL TENSILE STRESSES IN SiGe (IN KSI)

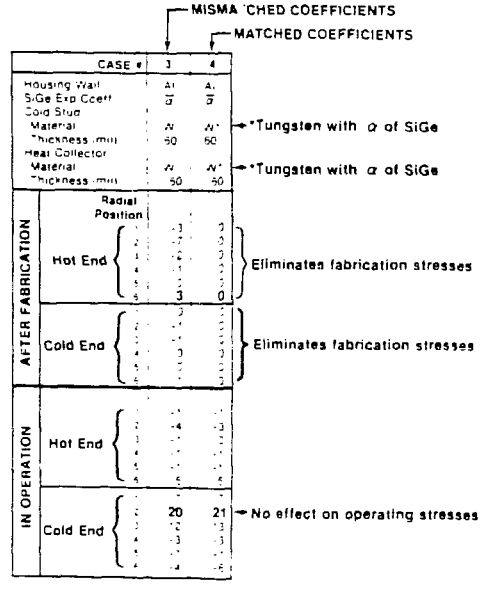

As would be expected, setting the expansion coefficients of the heat collector and cold stud equal to that of the SiGe legs eliminates all fabrication stresses, at both ends. But, as shown in Table 4, it has no significant effect on the high operating stresses.

5.3 Effect of Temperature Gradient

Having eliminated the bimetallic cold stud and the difference in expansion coefficients as the dominant cause of the high operating stresses at the cold end of the multicouple, we were left with two other possible explanations: the curvature of the SiGe leg assembly as the result of the 700°C temperature gradient; and the high expansion coefficient of the aluminum wall.

The first of these effects is illustrated in Figure 6, which shows what the stress-free deformation of the unbonded components would be at their operating temperatures. As can be seen, the SiGe assembly would assume a convex curvature at its upper (hot) surface and a concave curvature at its lower (cold) surface. The corresponding tungsten parts would, of course, remain flat.

Figure 6. Effect of Temperature Gradient on Unbonded Parts

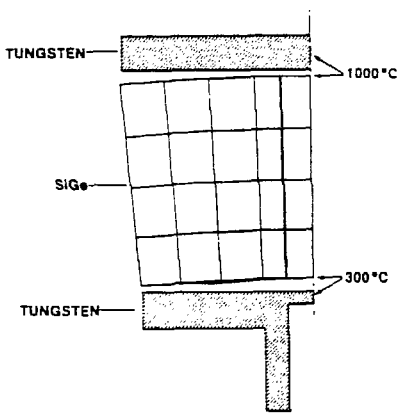

When the above parts are bonded together, the respective surfaces at each interface must remain congruent. Thus, there clearly is a conflict at each of the interfaces, resulting in tensile stresses near the outside of the hot interface and near the center of the cold interface. These theoretical stresses are qualitatively consistent with our earlier experimental observations. Thus, the observed stresses could in fact be due to the temperature gradient, even if the expansion coefficients of all the materials were identical.

To test whether this was the case, or whether the dominant stress source was the high expansion coefficient of the aluminum wall, the base-case multicouple was analyzed without any wall. The results of that analysis are displayed in Figure 7 and in Table 5.

Figure 7. Effect of Omitting Aluminum Wall from Base Case

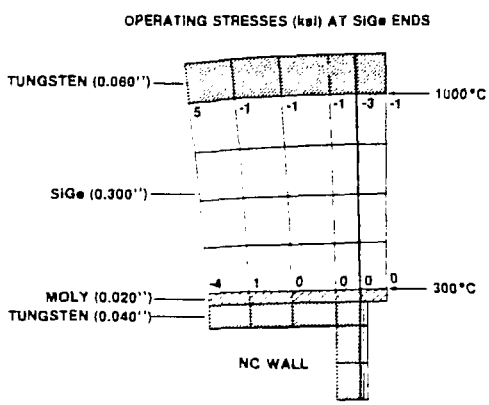

Table 5. Effect of Aluminum Wall
Axial Tensile Stresses in SiGe, in ksi

		MOUNTED ON WALL	WITHOUT WALL
CASE #		11	8
Housing Wall		Al	-
SiGe Exp Coeff		α(T)	α(T)
Cold Stud Material		W/Mo	W/Mo
Thickness (mil)		40/20	40/20
Heat Collector Material		W	W
Thickness (mil)		60	60
AFTER FABRICATION	Radial Position		
	Hot End 1		-3
	Hot End 2		-8
	Hot End 3		-2
	Hot End 4		-1
	Hot End 5		0
	Hot End 6		2
	Cold End 1		0
	Cold End 2		-2
	Cold End 3		-2
	Cold End 4		0
	Cold End 5		1
	Cold End 6		0
IN OPERATION	Hot End 1		-1
	Hot End 2		-3
	Hot End 3		-1
	Hot End 4		-1
	Hot End 5		-1
	Hot End 6		5
	Cold End 1		0
	Cold End 2		0
	Cold End 3		0
	Cold End 4		0
	Cold End 5		1
	Cold End 6		4

High operating stresses near center of cold end primarily due to aluminum wall

As can be seen, omission of the wall virtually eliminates the operating stress at the center of the multicouple's cold end. Thus, we conclude that the previously observed high stress at the center of the cold end was not due to the curvature of the leg assembly shown in Figure 6. Rather, it was due to the high expansion coefficient of the aluminum wall.

5.4 Wall Expansion Effect

To confirm this conclusion, we analyzed a case identical to the base case, except that the multicouple was bolted to a molybdenum wall, which matched the expansion coefficient of the cold stud. The results of that analysis are shown in Figure 8.

Figure 8. Base Case with Molybdenum Wall

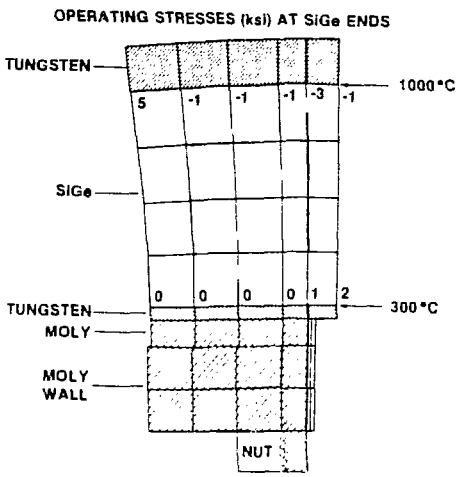

As can be seen, the high operating stresses near the center of the cold end virtually vanish when the expansion coefficient of the wall matches that of the cold stud.

These results confirm that the dominant stress source is the high expansion of the aluminum wall. The mechanism for this is clear from inspection of Figure 5. Near the axis of the multicouple, the expansion of the aluminum wall is resisted by the tension in the stud pin. But near the outside, the expansion of the aluminum causes the edges of the stud head to curve upward.

The resultant curvature of the stud surface is exactly opposite to the curvature of the leg assembly's cold end shown in Figure 6. Thus, the expansion of the aluminum wall causes a high operating stress at the center of the cold end, which led to the very serious cracks and cleavages observed in the initial tests.

It may legitimately be asked why the above analyses were not undertaken before the test hardware was built. In retrospect, they certainly should have been. But these analyses represent a major and time-consuming effort, and there was no a-priori evidence that they were needed, or that they would prove as informative and productive as they did.

6. Elimination of Thermal Stress

The principal cause of the thermal stresses having been determined, a number of possible design changes to eliminate those stresses were investigated. Some of these are discussed below:

6.1 Compliant Cushion

One possible solution would be to insert a low-modulus cushion between the cold stud and the SiGe assembly, to decouple the latter from the aluminum expansion effect. To this end, Thermo Electron — based on prior experience on another program — had recommended the addition of a thin graphite layer (Stackpole 2128) between the tungsten cold stud and the SiGe assembly. These two materials have very similar expansion coefficients, have been successfully bonded to each other, and the graphite has an attractively low modulus (~10^6 psi). When this suggestion was analyzed by Fairchild, it yielded the results shown in Figure 9 and Table 6.

Figure 9. Graphite-Cushioned Cold Stud

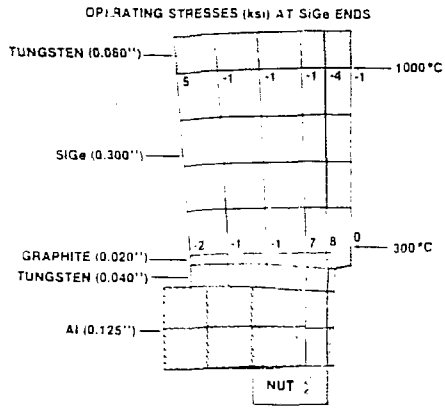

As can be seen, the graphite layer is quite compliant. As shown in Table 6, its use completely eliminates the cold-end fabrication stresses, and cuts the cold-end peak operating stress in half. While this was not considered good enough to ensure survival by itself, it was a big step forward and its use is beneficial in conjunction with other design improvements, as shown in Sections 6.2 and Reference [4].

Table 6. Effect of Graphite-Cushioned Cold Stud

MOLY STUD WITH TUNGSTEN COVER
TUNGSTEN STUD WITH GRAPHITE COVER

	CASE #	2	9	
	Housing Wall	Al	Al	
	SiGe Exp Coeff	$\alpha(T)$	$\alpha(T)$	
	Cold Stud:			
	Material	Mo/W	W/C	← △
	Thickness (mil)	40/20	40/20	
	Heat Collector:			
	Material	W	W	
	Thickness (mil)	60	60	
AFTER FABRICATION	Radial Position			
	Hot End 1	-4	-3	
	Hot End 2	-8	-7	
	Hot End 3	-3	-2	
	Hot End 4	2	-1	
	Hot End 5	0	0	
	Hot End 6	3	3	
	Cold End 1	1	0	
	Cold End 2	-2	0	
	Cold End 3	-3	0	
	Cold End 4	-2	0	
	Cold End 5	-2	0	
	Cold End 6	8	0	Graphite eliminates fabrication stresses
IN OPERATION	Hot End 1	-2	-1	
	Hot End 2	-5	-4	
	Hot End 3	-1	-1	
	Hot End 4	-1	-1	
	Hot End 5	-1	-1	
	Hot End 6	5	5	
	Cold End 1	8	0	
	Cold End 2	18	8	Operating stress lower,
	Cold End 3	10	7	but still too high
	Cold End 4	-5	-1	
	Cold End 5	-2	-1	
	Cold End 6	0	-2	

In addition to the graphite-cushioned cold stud, Thermo Electron had also suggested the use of a graphite heat collector, in place of the bimetallic (Mo/W) structure used in the initial test assemblies (see Figure 2). This suggestion was analyzed by Fairchild, with the results shown in Table 7.

Table 7. Effect of Equal-Thickness Graphite Heat Collector

	CASE #	11	12	
	Housing Wall	Al	Al	
	SiGe Exp Coeff	$\alpha(T)$	$\alpha(T)$	
	Cold Stud:			
	Material	W/Mo	W/Mo	
	Thickness (mil)	40/20	40/20	
	Heat Collector:			
	Material	W	C	← △
	Thickness (mil)	60	60	
AFTER FABRICATION	Radial Position			
	Hot End 1	-3	0	
	Hot End 2	-8	-1	
	Hot End 3	-2	0	
	Hot End 4	-1	0	
	Hot End 5	0	0	
	Hot End 6	2	0	
	Cold End 1	0	0	
	Cold End 2	-2	-1	
	Cold End 3	-2	-1	
	Cold End 4	0	0	
	Cold End 5	-1	0	
	Cold End 6	0	0	
IN OPERATION	Hot End 1	-1	0	
	Hot End 2	-4	-2	
	Hot End 3	-1	0	
	Hot End 4	-1	0	
	Hot End 5	-2	0	
	Hot End 6	5	0	← For same thickness (0.060"), graphite heat collector eliminates high operating stress at outside of hot end
	Cold End 1	7	8	
	Cold End 2	18	18	
	Cold End 3	12	12	No change at cold end
	Cold End 4	-4	-4	
	Cold End 5	-1	-1	
	Cold End 6	-5	-5	

As can be seen, the operating tensile stresses at the multicouple's hot end would be completely eliminated by the use of a graphite heat collector of equal thickness as before. However, this conclusion is somewhat misleading, because in reality a graphite heat collector must be almost three times as thick, as explained in Section 6.3.

6.2 Double-Headed Cold Stud

Another design change, suggested by Fairchild, was the use of a double-headed cold stud, illustrated in Figure 10.

Figure 10. Double-Headed Cold Stud Design

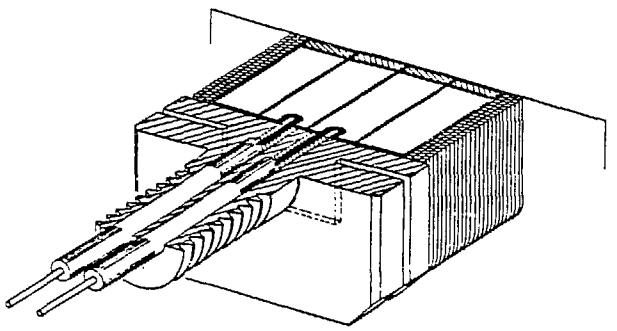

As shown, one of the stud heads is bonded to the SiGe thermopile, while the other bears against the aluminum housing wall. The intervening stress-relief slots (from all four edges) effectively serve to isolate the thermopile from the effects of the aluminum wall expansion.

However, the slots shown in Figure 10 impede not only stress transmission but also heat transmission. This is illustrated in Figure 11, which shows the temperature distribution for a typical design.

Figure 11. Temperature Map (in °C) of Double-Headed Cold Stud

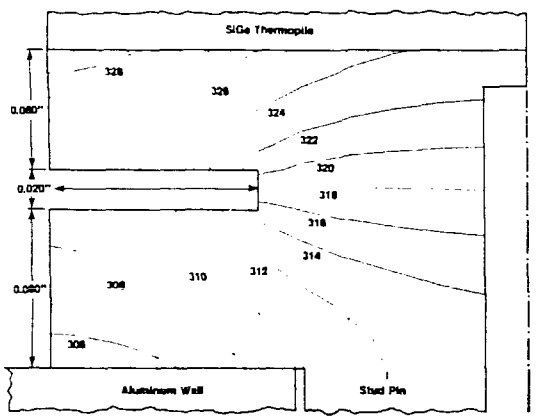

As can be seen, the temperature drops for the dimensions shown in Figure 11 are considerable but not prohibitive. Therefore, these dimensions were tentatively selected for the stress analysis required to evaluate the merit of the concept.

Again, symmetry conditions were invoked to limit the stress-analysis model to a 45° segment. The computed results for a 0.060" heat collector and an all-tungsten double-headed cold stud are presented in Figure 12 and Table 8.

The effectiveness of the stress relief slots in isolating the SiGe legs from the aluminum expansion effects are clearly shown by the deflection plots. As can be seen, the edges of the lower stud head curve upward, as the result of the aluminum expansion; while those of the upper stud head curve downward, as the result of the SiGe temperature gradient.

Figure 12. Effect of Double-Headed Tungsten Stud Operating Stresses at SiGe Ends, in ksi

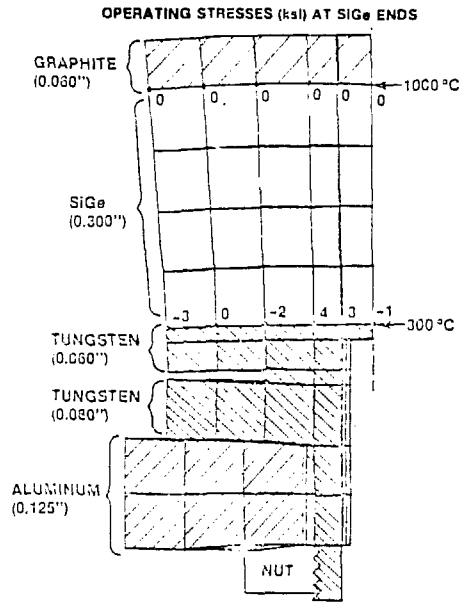

Table 8 compares the cold-end stresses for single-headed and double-headed cold studs. As can be seen, the double-headed stud has slightly higher fabrication stresses, as the result of its greater thickness and stiffness. But its peak operating stress is only one fifth that of the single-headed stud.

Table 8. Comparison of Single-Headed and Double-Headed Tungsten Studs

AXIAL TENSILE STRESSES IN SiGe, IN ksi

		SINGLE	DOUBLE	
CASE #		3	19	
Housing Wall		Al	Al	
SiGe Exp Coeff		$\bar{\alpha}$	$\bar{\alpha}$	
Cold Stud:				
Material		W	W	
Thickness (mil)		60	60/80	←Δ
Heat Collector:				
Material		W	C	←Δ
Thickness (mil)		60	60	
AFTER FABRICATION	Radial Position			
	Hot End 1	-3	0	
	Hot End 2	-7	-1	
	Hot End 3	-2	0	
	Hot End 4	-1	0	
	Hot End 5	0	0	
	Hot End 6	3	0	
	Cold End 1	0	0	
	Cold End 2	-1	0	
	Cold End 3	-1	0	
	Cold End 4	0	-1	
	Cold End 5	0	0	
	Cold End 6	1	2	←Increased thickness and stiffness at center of double-headed stud results in somewhat higher fabrication stress
IN OPERATION	Hot End 1	-1	0	
	Hot End 2	-4	0	
	Hot End 3	-1	0	
	Hot End 4	-1	0	
	Hot End 5	-1	0	
	Hot End 6	5	0	
	Cold End 1	7	-1	
	Cold End 2	20	3	Double-headed stud yields much lower operating stress at cold end
	Cold End 3	12	4	
	Cold End 4	-3	-2	
	Cold End 5	-1	0	
	Cold End 6	-4	-3	

Thus, we see that the double-headed stud is much more effective than the graphite cushion in reducing the operating stresses at the center of the cold end. The effect of combining both of those design improvements is illustrated in Figure 13.

Replacing 0.020" of the 0.060" upper stud head with graphite lowers the fabrication stress from 2 ksi to 1 ksi; and, as shown in Figure 13, it reduces the peak cold-end stress from 4 ksi to 2 ksi.

Figure 13. Double-Headed Tungsten Cold Stud with Graphite Cushion

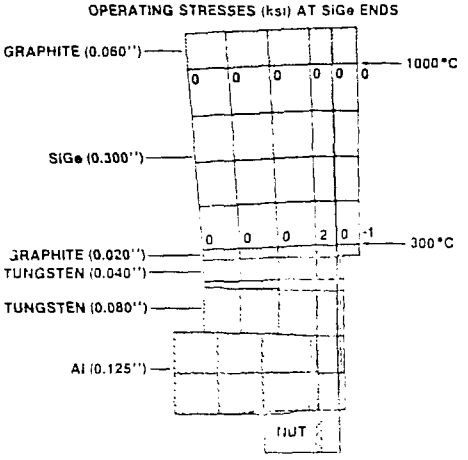

Additional analysis showed that even that value can be further cut in half by using 0.040" of graphite instead of 0.020". Thus, theory predicts that the combination of the double-headed stud with the compliant graphite cushion would virtually eliminate the cold-end stresses.

6.3 Graphite Heat Collector

As suggested earlier, a heat collector maximum thickness of 0.060" is adequate for molybdenum but not for graphite. The thermal conductivity of the graphite used (Stackpole 2128) at 1000°C is 0.43 w/cm°C, versus 1.15 w/cm°C for molybdenum. Thus, a graphite heat collector must be about 2.5 times as thick for the same thermal effectiveness. But since its density is only one sixth that of molybdenum, a graphite heat collector has less than half the weight of an equivalent molybdenum heat collector.

In addition to its lower weight and greater compliance, a graphite heat collector has three other advantages over molybdenum: It is easier to machine. It avoids the need for the troublesome W/Mo joint discussed in Section 4 of Reference [2]. And it avoids the need for a high-emissivity coating, since the emissivity of graphite is inherently high. Such a coating, which must last for at least seven years at operating temperature, would have been required in the case of a molybdenum heat collector, to avoid excessive heat source temperatures.

In fact, the heat source is constrained to a maximum surface temperature of 1100°C, and this constraint dictates the required heat collector thickness profile. To determine the optimum thickness profile, Fairchild conducted an iterative series of three-dimensional thermal analyses. The minimum-weight solution for the prescribed heat flow and boundary temperatures is depicted in Figure 14.

The optimum heat collector has the shape of a very shallow pyramid or pagoda. The variation of its thickness z as a function of its x and y dimension is indicated by the thermal-model plot in Figure 14. (Note the difference in scale.)

Figure 14. Isotherm Map of Graphite Heat Collector with Optimized Thickness Profile

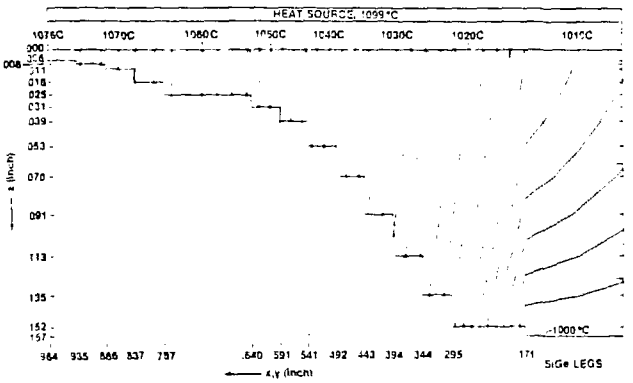

As shown, the resultant isotherms are fairly evenly spaced, which demonstrates that the shape is close to optimum. However, they are very widely spaced near the center, above the SiGe legs. This indicates that we have more graphite than needed in this region.

Figure 14 shows a maximum heat collector thickness of 0.157", compared to the previously used 0.060" value. To determine the effect of a thicker heat collector on the hot-end stresses, the case illustrated in Figure 13 was rerun with a 0.180" heat collector, with the results shown in Figure 15.

Figure 15. Effect of 0.180" Graphite Heat Collector

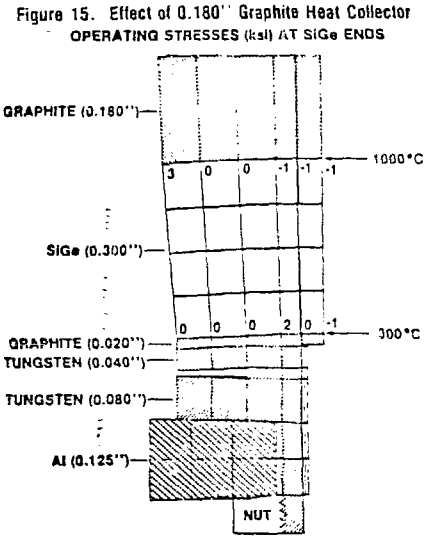

Comparison of Figures 13 and 15 shows that increasing the heat collector thickness from 0.060" to 0.180" has no effect on the cold-end stresses, but produces an operating tensile stress of 3 ksi at the outer corner of the hot end. This is due to the increased stiffness of the thicker graphite plate. The stiffer heat collector resists conforming to the gradient-induced curvature of the thermopile shown in Figure 6. This results in compressive stresses near the center and tensile stresses at the outside of the interface. Thus, the replacement of W/Mo by an equivalent thickness of graphite has eliminated the fabrication stress at the hot end and has reduced the peak operating stress from 5 ksi to 3 ksi, but has not eliminated it.

While the remaining 3 ksi stress may be tolerable, Fairchild suggested that this could be further reduced by cutting radial slots into the heat collector at 45° intervals. This would have no effect thermally,

but would make it easier for the heat collector to bend and to conform to the curvature of the thermopile caused by the temperature gradient.

To determine whether this would in fact reduce the tensile stress at the hot end's outer corner, the case illustrated in Figure 15 was modified analytically by assuming 45° slots penetrating the full thickness of the heat collector. The effect of this slotting is shown in Table 9.

Table 9. Effect of Slotting Graphite Heat Collector

		UNSLOTTED	SLOTTED	
CASE #		18	28	
Housing Wall		Al	Al	
SiGe Exp Coeff		$\alpha(T)$	$\alpha(T)$	
Cold Stud: Material		W/W/C	W/W/C	
Cold Stud: Thickness (mil)		80/40/20	80/40/20	
Heat Collector: Material		C	C	
Heat Collector: Thickness (mil)		180	180*	*Slotted at 45° intervals
AFTER FABRICATION	Radial Position			
	Hot End 1	0	1	
	Hot End 2	0	0	
	Hot End 3	0	0	
	Hot End 4	0	0	
	Hot End 5	0	0	
	Hot End 6	1	0	
	Cold End 1	0	0	
	Cold End 2	0	0	
	Cold End 3	0	0	
	Cold End 4	0	0	
	Cold End 5	0	0	
	Cold End 6	1	1	
IN OPERATION	Hot End 1	−1	2	← New Stress Near Center
	Hot End 2	-1	0	
	Hot End 3	-1	0	
	Hot End 4	0	0	
	Hot End 5	0	0	
	Hot End 6	3	1	← Corner Stress Much Reduced
	Cold End 1	-1	-1	
	Cold End 2	0	0	
	Cold End 3	2	2	
	Cold End 4	0	0	
	Cold End 5	0	0	
	Cold End 6	0	0	

As can be seen, slotting the 0.180"-thick heat collector reduces the operating stress at the hot end's corner from 3 ksi to 1 ksi, but produces a tensile stress of 2 ksi at the center. However, Fairchild suggested that this 2 ksi stress could be reduced by slotting the heat collector to less than its full thickness, as illustrated by the dashed line in Figure 16; and by adding a countersink hole at the center of its hot surface, as illustrated by the solid line.

Figure 16. Isotherm Map of Graphite Heat Collector with Optimized Thickness Profile

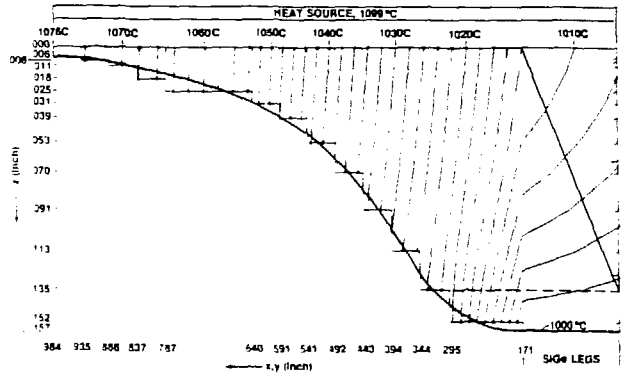

The reason for the countersink hole is that there is more graphite near the center of the heat collector than is needed. Removing this unneeded material by countersinking does not significantly affect the temperature distribution, but does lighten the heat collector and reduce its stiffness, thereby reducing the hot-end SiGe stresses. As shown in Figure 17, a multicouple with a graphite heat collector incorporating the suggested slots and countersink has been built by Thermo Electron, and is undergoing evaluation tests.

Figure 17. Graphite Heat Collector

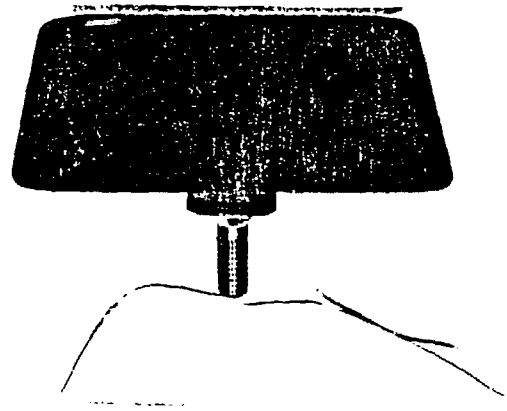

6.4 Vibration Test

The above analyses indicate that the use of a graphite cushion and graphite heat collector is beneficial in reducing thermal stresses in the SiGe thermopile. This makes it important to determine whether the graphite components can, in fact, be bonded to their neighbors; and whether these components and their neighbors will survive the predicted launch vibration loads.

To help answer these questions, Thermo Electron fabricated a multicouple with a graphite cushion and heat collector, as illustrated in Figure 18. To bond the thermopile to the heat collector, its contact area was first coated with a 0.004"-thick layer of CVD tungsten. This was then bonded to the SiMo hot shoes by means of a high-temperature (1100°C) glass layer, as in previous multicouples. In the case of the cold-end graphite cushion, no tungsten coating was required, since the low-temperature glass (680°C) was found to wet the graphite well. The lower face of the graphite cushion was bonded to the tungsten stud by means of a Nioro braze joint.

Figure 18. Multicouple with Graphite Components, for Performance and Vibration Tests

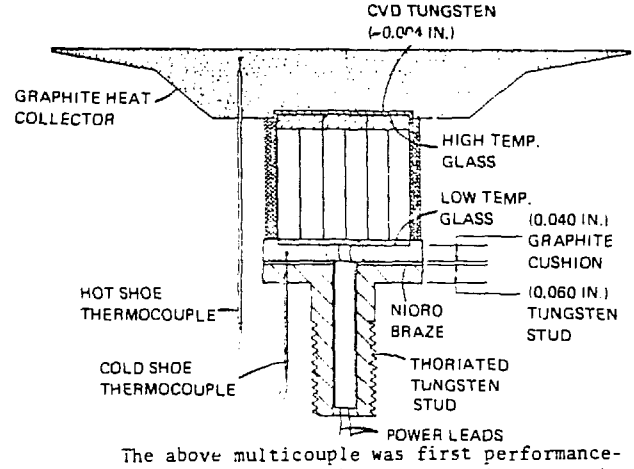

The above multicouple was first performance-tested (at design temperature) at Thermo Electron, then vibration-tested at Fairchild, and then performance-tested again at Thermo Electron. As can be seen, the multicouple employed a single-headed cold stud. To

avoid the previously observed thermal stresses due to the aluminum wall expansion, the multicouple was tested without any wall. Instead, it was cooled by clamping a chill block directly to the stud pin. Its performance was found to be good, both before and after the vibration test, with no significant degradation.

In the flight generator, the launch loads on the multicouple are not only those due to its own weight, but also those due to the weight of the multifoil insulation package, which is substantial. The multifoil insulation is supported only by the multicouples in the flight generator. During launch, this can result in significant additional shear loads and tensile loads on the SiGe thermopile and on the heat collector bond.

To simulate this effect, the vibration test designed by Fairchild employs a 2 x 3 multicouple array, supporting a corresponding multifoil package, as shown in Figure 19. Five of those multicouples are dummies, to simulate the foil support provided by neighboring elements. Only one (of the two middle ones) is a real multicouple.

Figure 19. Multicouple Vibration Test Fixture

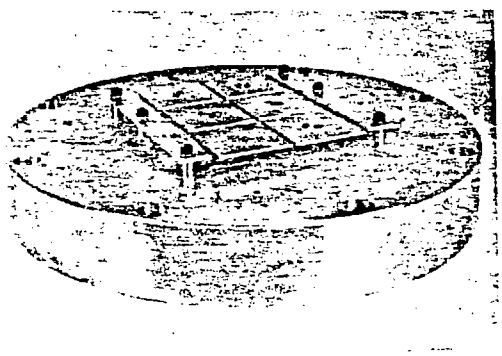

The multicouple depicted in Figure 18 was subjected to 2-minute random-vibration tests on three axes, based on currently predicted levels for the shuttle-launched Galileo and ISPM missions. Each of the three directions was subjected to an 8.11 grms acceptance test and a 14.2 grms qualification test. In addition, the z-direction (parallel to the multicouple axis) was subjected to a 22.6 grms overtest. The power spectrum for that test is depicted by the jagged curve in Figure 20.

Figure 20. Multicouple Vibration Spectrum in 22.6 Grms Test

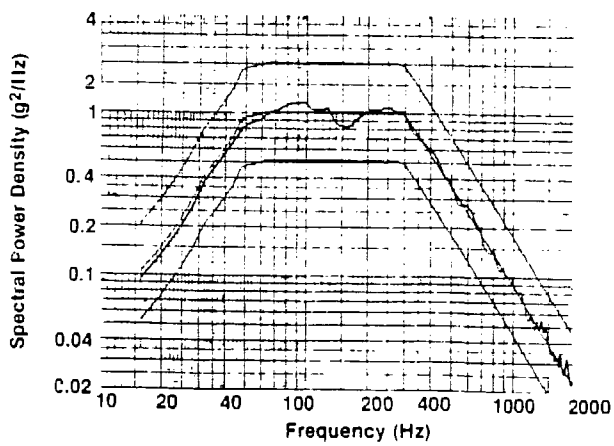

No damage was observed in the above tests, except for some minor fracture at the thin corner of the graphite heat collector. This can be avoided by truncating the corners in future heat collectors, without significant effect on multicouple performance. The in-gradient electrical performance of the tested multicouple was unchanged by the vibration test.

7. Summary

The analysis described in this paper has identified the causes of the thermal-stress problems revealed by the preceding tests. The principal problem was shown to be the result of the high expansion coefficient of the aluminum housing wall. To alleviate these problems, the paper described a number of design changes, including the use of a double-headed stud with a 0.040" graphite cushion at the multicouple's cold end, and the use of a graphite heat collector with stress-relief slots at its hot end. The combined effect of these changes is summarized in Table 10.

Table 10. Total Improvement Over Base Case
Axial Tensile Stresses in SiGe, in ksi

			BASE CASE	COMBINED IMPROVEMENTS	
		CASE #	1	25/28	
		Stud Head	Single	Double	←△
		Housing Wall	Al	Al	
		SiGe Exp Coeff	α(T)	α(T)	
		Cold Stud Material	Mo/W	W/W/C	←△
		Thickness (mil)	40/20	80/20/40	←△
		Heat Collector Material	W	C	←△ *Slotted at 45° intervals
		Thickness (mil)	50	190	←△
AFTER FABRICATION	Radial Position				
	Hot End	1	-3	1	
		2	-8	2	
		3	-3	0	
		4	-2	0	
		5	2	0	
		6	3	0	←Fabrication stress at hot corner eliminated
	Cold End	1	1	0	
		2	-3	0	
		3	-3	0	
		4	-2	0	
		5	2	0	
		6	7	1	← High fabrication stress at cold corner very much reduced
IN OPERATION	Hot End	1	-2	2	← Options for reducing stress at center exist
		2	-5	0	
		3	-1	0	
		4	-2	0	
		5	-2	0	
		6	5	1	← High operation stress at hot corner greatly reduced.
	Cold End	1	8	0	← Very high operating stress near center of cold end largely eliminated
		2	17	0	
		3	10	1	
		4	-5	-0	
		5	-3	0	
		6	0	0	

As can be seen, these design changes have virtually eliminated the previous fabrication stresses at the hot and cold corners, the previous operating stress at the hot corner, and the extremely high operating stress at the center of the cold end. Alternative solutions for relieving these and some other problems are described in the next paper [4].

Acknowledgment

The author takes pleasure in acknowledging that the work described here reflects the contributions of many individuals including (alphabetically): M. Eck, F. Kline, H. Kling, M. Mukunda, and J. Newell of Fairchild, and K. Hagen, F. Huffman, and V. Rang of Thermo Electron.

REFERENCES:

[1] A. Schock, "Modular Isotopic Thermoelectric Generator", Proceedings of the 1981 IECEC, Volume 1, Pg. 327.

[2] A. Schock, "MITG Test Assembly Design and Fabrication", Proceedings of the 1983 IECEC, previous paper.

[3] M. Eck, M. Mukunda, "MITG Test Procedure and Results", Proceedings of the 1983 IECEC, preceding paper.

[4] A. Schock, "Revised MITG Design, Fabrication Procedure, and Performance Predictions", Proceedings of the 1983 IECEC, next paper.

[5] J. Newell, "Structural Analysis of a Thermoelectric Generator Element", MSC/NASTRAN User's Conference, Pasadena, California, March 1983.

DISCLAIMER